Available online at www.sciencedirect.com
SCIENCE DIRECT®
Biomaterials 26 (2005) 7504–7513
Biomaterials
www.elsevier.com/locate/biomaterials

Effect of sample geometry on the apparent biaxial mechanical behaviour of planar connective tissues

Stephen D. Waldman[a,*], J. Michael Lee[b]

[a]Department of Mechanical and Materials Engineering, Queen's University, McLaughlin Hall, Room 205, 130 Stuart Street, Kingston, Ont., Canada K7L 3N6
[b]School of Biomedical Engineering, Dalhousie University, 5981 University Avenue, Room 2115, Halifax, NS, Canada B3H 3J5

Available online 5 July 2005

Abstract

Mechanical testing methodologies developed for engineering materials may result in artifactual material properties if applied to soft planar connective tissues. The use of uniaxial tissue samples with high aspect ratios or biaxial samples with slender cruciform arms could lead to preferential loading of only the discrete subset of extracellular fibres that fully extend between the grips. To test this hypothesis, cruciform biaxial connective tissue samples that display distinctly different material properties (bovine pericardium, fish skin), as well as model textile laminates with predefined fibrous orientations, were repeatedly tested with decreasing sample arm lengths. With mechanical properties determined at the sample centre, results demonstrated that the materials *appeared* to become stiffer and less extensible with less slender sample geometries, suggesting that fibre recruitment increases with decreasing sample arm length. Alterations in the observed shear behaviour and rigid body rotation were also noted. The only truly reliable method to determine material properties is through in vivo testing, but this is not always convenient and is typically experimentally demanding. For the in vitro determination of the biaxial material properties, appropriate sample geometry should be employed in which all of the fibres contribute to the mechanical response.

Keywords: Biaxial; Mechanical testing; Sample geometry; Pericardium; Skin; Artifacts

1. Introduction

The mechanical characterization of planar connective tissues (e.g. pericardium) is of particular interest for physiology and for the design of bioprosthetic replacements. The bulk of this information has been obtained through in vitro testing since the determination of mechanical properties in vivo can be extremely difficult. These in vitro observations are then routinely used as predictors of material performance in situ with the inherent assumption that the testing methodology has not influenced the observed behaviour. Nevertheless, the geometry of the sample and the method of gripping the sample edges may have profound effects on any measured mechanical properties since they directly influence how the load is transferred to the underlying fibrous network. Although these issues are believed to be important, they have been essentially ignored for the biaxial mechanical testing of connective tissue materials.

Historically, two methods have been used to determine biaxial mechanical properties of planar connective tissues: inflation studies [1–3] and the deformation of square specimens with sutured edges [4–9]. Hildebrant et al. [1] first reported the inflation method in which a circular portion of tissue was clamped and one side was subjected to a positive pressure in order to deform the membrane. The other, and arguably more popular method of biaxial testing has been the use of square samples with sutured edges based on the work of Lanir

*Corresponding author. Tel.: +1 613 533 2896; fax: +1 613 533 6489.
E-mail addresses: waldman@me.queensu.ca (S.D. Waldman), jmlee@is.dal.ca (J.M. Lee).

0142-9612/$ - see front matter © 2005 Elsevier Ltd. All rights reserved.
doi:10.1016/j.biomaterials.2005.05.056

and Fung [4]. Interestingly, none of these works have made mention of the vast literature regarding biaxial testing of engineering materials. The most popular sample geometry for the biaxial testing of engineering materials has been the cruciform (cross-shaped) sample developed by Mönch and Galster [10]. This geometry has been extensively used in the testing of metallic materials [11–13] and composite materials [14–17]. Recent studies on fabric [18] and planar connective tissues [19,20] have also used similar sample geometries.

Although not explicitly mentioned by Mönch and Galster [10], the adaptation of long sample arms to biaxial testing is loosely based upon the work of the French mathematician and engineer Adhémar Barré de Saint-Venant (1797–1886). Saint-Venant's principle essentially states that stress (and presumably the strain) distribution may be assumed to be independent of the actual mode of load application—except in the immediate vicinity of where the load is applied. The method of gripping sample edges imposes local stresses and strain constraints at the grip-sample interface and these local influences are considered to become negligible at some distance away from the grip. The Saint-Venant principle has thus been the primary motivation for the use of long slender samples in uniaxial material testing, with extensometer-based strain measurement at the sample mid-region.

Previous studies have demonstrated the Saint-Venant effect in uniaxial connective tissue samples [21,22], stating that strain measurements based on the grip-to-grip displacement may grossly overestimate the specimen strain and suggested measurement of local strains at the sample centre. Jimenez et al. [23] also demonstrated negligible influence of the grips on central specimen strains when the tendon sample length was greater than eight diameter multiples: a ratio similar to the aspect ratio (ratio of sample length to width) used when testing engineering materials.

In connective tissues subjected to tensile loads (e.g. tendon, pericardium, etc.), the extracellular reinforcing fibres are presumably orientated along lines of principle stresses or strains to effectively distribute the load throughout the structure. Observations of these fibres in the pericardium [24–28] and fish skin [29,30] at a light microscopic level (100–200X magnification) reveal continuous bands or sheets of collagen fibrils with interspersed elastic fibres that also appear to be continuous in nature. However, there is some evidence that collagen fibrils in fish skin [31] as well as in tendons and ligaments are not continuous but display a spectrum of characteristic lengths [32–34]. If collagen fibrils are in fact discontinuous, then there must be some level of continuity within the structure in order to distribute the applied load since the amorphous matrix likely does not mediate stress transfer between adjacent fibrils [35]. Although certain proteoglycans bind specifically to collagen [36] it is unlikely that their relatively long filaments are completely responsible for holding the entire structure together. The more plausible explanation is that physical interactions between the adjacent fibrils, such as interweaving [35] is the predominant mechanism by which load is transmitted throughout the tissue. Therefore, either these tissues exhibit continuous fibre reinforcement, or it can be assumed that an "effective" continuous fibre reinforcement exists at some level within the tissue.

This continuous nature of the reinforcing fibres in planar connective tissues may lead to unanticipated difficulties when attempting to ascertain the mechanical properties of these tissues by conventional testing methods. The use of uniaxial samples with high aspect ratios or biaxial samples with slender cruciform arms could lead to the situation where a discrete subset of fibres that fully extend from grip-to-grip are preferentially loaded—especially if the fibres are not completely aligned with the testing axes. This subset of fibres is dependent on the aspect ratio of the specimen and the orientations of the fibre populations. By altering sample geometry to reduce the influence of the grips, the problem of loading a smaller proportion of the reinforcing fibres may be exacerbated. Therefore, any measured mechanical properties are to some extent artifactual, with properties reflecting sample geometry. There have been a few studies that reported alterations in mechanical behaviour with varying sample length or aspect ratio [37,38]; unfortunately these studies based their strain measurements on the grip-to-grip displacement and their conclusions must be viewed with caution.

The purpose of this study was to test the hypothesis that, as the length of the sample arms are reduced, an *apparent* increase in stiffness (tangent modulus) and decrease in extensibility (maximum strain) of the material sample will occur presumably due to an increasing proportion of collagen fibres that fully extend between the grips. Equibiaxial tension experiments were undertaken on both pericardial heart valve materials and fish skin: two planar connective tissues that have different structures and display distinctly different material properties. After testing of connective tissue samples, similar experiments were performed on model textile laminates with simultaneous measurement of fibre orientation during deformation to help determine the underlying mechanism responsible.

2. Methods

2.1. Materials

Three different materials were used in this study: (i) fish skin which exhibits a simple orthogonal array of collagen fibres [31,39], (ii) bovine pericardium which displays a more complex

interwoven, laminar collagen fibre architecture [24,40,41], and (iii) model textile laminates with predefined fibre orientations.

Fresh haddock (*Melanogrammus æglefinus*) were obtained within 3 days of catch (on ice) from a local distributor. The intact skin was descaled and a portion of the ventral surface was excised adjacent to the pectoral fin, immediately below the midline. Any adherent muscle was then removed from the excised skin sections. Biaxial skin samples were aligned along the head–tail and dorsal–ventral axes.

Intact bovine pericardia were obtained from 1–2 year old cattle immediately after slaughter. The left ventral surface was stripped of any adherent fat and the base-to-apex direction was marked with two reference sutures: one placed at the aortic root and the other at the apex of the heart. A portion of the parietal pericardium immediately over the left ventricle was excised and biaxial samples were aligned in the base-to-apex and circumferential directions.

Model textile materials were comprised of laminated, unwoven, braided black polyester fibres embedded in a translucent latex rubber matrix (Woodland Scenics, Linn Creek, MO). The two layer laminates had initial fibre directions aligned at orthogonal angles. The textile laminates had a fibre volume fraction of $15.3 \pm 0.5\%$ and a fibre linear density of 2.78 ± 0.03 fibres/mm ($n = 16$). Biaxial model textile material samples were cut to create nominal fibre directions of 15° and 105° to the testing axes to simulate the the connective tissues used in the study which have collagen fibres oriented slightly off-axis to the anatomical directions. Actual initial fibre directions were measured at $16.5 \pm 0.3^\circ$ and $105.6 \pm 0.2^\circ$ ($n = 24$), respectively.

All sample thickness measurements were preformed using a non-rotating Mitutoyo thickness gauge (Mitutoyo Corporation, Tokyo, Japan) [42]. The recorded thickness value for each sample was the average taken from four random locations throughout the sample area.

2.2. Sample preparation and mechanical testing

All samples were cut into cross shapes with 20 mm wide arms (reflecting the median sample width used in previous studies), mounted in parallel-plate sandwich grips lined with water-proof sandpaper and repeatedly tested with decreasing arm lengths (Fig. 1). Three different grip-to-grip arm lengths were used: (i) 60 mm, (ii) 44 mm, and (iii) 22 mm. The 22 mm cross thus represented an approximation to a clamped square sample in which all of the fibres should be contained between the grips. Biaxial testing was conducted using an MTS (Minnesota, MN) servo-hydraulic biaxial test device equipped with four actuators and phased stroke/load waveform synthesis [20]. Samples were preloaded to 0.5 g/axis, which was subsequently defined as the zero strain state. Materials were cyclically deformed (to precondition the sample) with a haversine waveform under stroke control at 1 Hz for 30 cycles. Actuator displacements were set to achieve defined peak equibiaxial loads: fish skin 100 g/axis, pericardium 200 g/axis [20], and model materials 400 g/axis (due the different extensibilities of the sample materials). Model textile materials were tested in air at room temperature whereas connective tissues were tested in a fluid medium maintained at a specified temperature: fish skin samples were tested in distilled water at room temperature (due to temperature limitations of the testing apparatus) and pericardial samples were tested in Hanks' solution at $37\,^\circ$C [20]. The following number of samples were tested for each material: fish skin ($n = 16$), bovine pericardium ($n = 8$) and model textile laminates ($n = 8$).

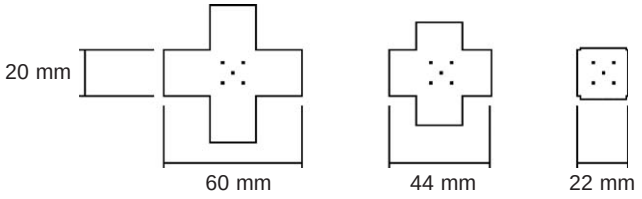

Fig. 1. Three cruciform sample geometries were used in this study along with the locations of the surface markers used to determine the biaxial strain field. All samples had an arm width of 20 mm and the three grip-to-grip arm lengths were 60, 44, and 22, respectively (indicated below each sample).

Generalized large deformation biaxial strain fields were quantified at the sample centre through video tracking of surface deformation markers. Five particles of sand (nominal diameter 300 μm) were arranged in a central square array (~10 mm in width) with one additional marker at the geometric centre of the sample. Markers were attached to the sample surface with a small amount of cyanoacrylate glue (Elmer's Productions Canada Inc., Brampton, Ont.). For the model materials, small droplets of Liquid Paper™ (The Gillette Company, Boston, MA) diluted with toluene were used as the surface deformation markers (nominal diameter 300 μm). Video images were collected with an overhead CCD camera (Cohu 5000, San Diego, CA), an 8-bit grayscale video acquisition board (Scion Corporation LG-3, Frederick, MD), and image analysis software (NIH Image 1.61, US National Institutes of Health) on a Macintosh computer (Centris 650, Apple Computer Inc., Cupertino, CA). Resulting load-time behaviour was collected using a 12-bit A/D acquisition board (National Instruments NB- MIO-16X, Austin, TX) and LabVIEW 2.2.1 data acquisition software (National Instruments, Austin, TX) on another Macintosh computer (PowerMac 7200, Apple Computer Inc., Cupertino, CA). Both analog data acquisition and video capturing were collected at 30 Hz and synchronized by a digital pulse generated by the MTS biaxial device to collect only the last three cycles of the 30 cycle loading regimen.

2.3. Data analysis

Particle position histories were determined from subsequent analysis of captured video images. The position of a particle was defined as the geometric centre of a "best fit" ellipse placed around the particle. The deformation gradient was determined from the surface marker displacement histories using an isoparametric (4-noded) finite element procedure [43,44] calculated at the fifth node placed at the geometric centre of the sample. The associated Green strain and Kirchhoff stress tensors were determined from the deformation gradient [45,46]. This procedure has been well described by others [7–9]. Calculation of the deformation gradient and corresponding stress and strain tensors were performed using

mathematical analysis software (Mathematica 3.0, Wolfram Research, Champaign, IL).

The last three stress–strain cycles were then averaged and the following parameters were determined from this average cycle: (i) maximum stresses and strains (extensiblity), (ii) tangent modulus (stiffness), (iii) maximum rigid body rotation and, in addition for the model materials, (iv) maximum fibre angular rotations (see below). The maximum stress and strain components were defined as the difference between the values measured at the valley and peak in the average deformation cycle. The three-cycle-averaged stress–strain curves were also interpolated at incremental levels of stress (5 kPa) to calculate the tangent modulus, which was defined as the slope of the average stress–strain curve calculated from a second-order central-difference numerical derivative. The rigid body rotation of the sample centre was calculated from a polar decomposition of the deformation gradient [47]. Rotation data was least-squares curve fitted to a generalized sinusoidal function and the maximum rigid body rotation was then defined as twice the value of the calculated amplitude. Note that the measured shear behaviour and rigid body rotation are separate phenomena since the shear strains were corrected for rigid body rotation during the analysis.

2.4. Measurement of fibre orientation

Fibre orientations for model textile materials during deformation were measured using an image analysis technique known as the Hough Transform [48]. This transform estimates the parameters of straight lines (slope and intercept) within an image from the locations of individual pixels. First, consider the equation of an arbitrary straight line in Cartesian image space (x, y):

$$y = mx + b, \tag{1}$$

where, m is the slope of the line and b is the intercept on the y axis. In Eq. (1), x and y are the coordinate values of any point on the line, and m and b represent the parameters of the line. Rearranging Eq. (1) in terms of the slope and intercept yields:

$$m = -\frac{1}{x}b + \frac{y}{x}. \tag{2}$$

Eq. (2) also represents a straight line in Cartesian parameter space (m,b), where m and b are now the coordinate values and x and y are now constants. Using this relationship, any point (x,y) in image space corresponds to a straight line in parameter space. If a straight line within an image is comprised of numerous points, these points then correspond to a family of lines in parameter space which intersect at a single location: the slope and intercept of the original line (Fig. 2). The transformed image, in parameter space, is a plot in which the number of pixels that are contained within all possible lines occurring in the original image are plotted versus slope and intercept (the vertical and horizontal axes of the plot, respectively). Since the transformed images are two-dimensional, the numbers of pixels within the original lines are represented by an equivalent grey-scale value (i.e. the darker features in the transformed image refer to lines within the original image that were comprised of numerous pixels). Since the lines to be detected typically contain a vast number of pixels, the transformed image can be thresholded to filter out these particular lines from all of the remaining others. It should be mentioned that, in the image space, the polar form (ρ,θ) of the line is routinely used instead of the Cartesian form (x,y) to avoid problems with lines that are nearly vertical.

For the model textile materials, the captured video images were used to measure the dynamic fibre orientations during mechanical stretch. Average fibre orientations for each fibre population were determined within the central region of the sample bounded by the surface deformation markers (Fig. 2). Original images were digitally enhanced to isolate the underlying fibres prior to applying the transformation by adjusting the contrast and removing the image background using a 2D Rolling Ball algorithm (NIH Image 1.61, US National Institutes of Health). Transformed images were also similarly enhanced prior to thresholding. Maximum fibre angular rotation during deformation was determined in the same manner as the rigid body rotation: rotation data was least-squares curve fitted to a generalized sinusoidal function and the maximum angular rotation was defined as twice the value of the calculated amplitude.

2.5. Statistics

All calculated deformation parameters were analyzed using repeated-measures ANOVA statistics (SuperANOVA and StatView 4.1, SAS Institute, San Francisco, CA). The "within subject" effect (i.e. specific differences between sample arm length groups) was analyzed using least-square mean contrasts. The minimum level of significance was associated with p-values less than 0.05.

3. Results

The *apparent* mechanical properties of all materials, determined at the sample centre, were found to change with sample geometry. Generally, samples appeared to be stiffer and less extensible with decreasing arm length. Altered shear behaviour and rigid body rotation were also observed upon the change in sample arm length. The magnitude of the maximum shear stress and strain, as well as the rigid body rotation, was observed to decline with decreasing arm length.

3.1. Fish skin

The fish skin samples exhibited strongly anisotropic behaviour in which the dorsal–ventral axis was stiffer than the head-tail axis. This caused the dorsal–ventral axis to display low magnitude compressive strains under the imposed equibiaxial tensile loads with no measurable tensile strains observed throughout the deformation cycle. Although not common in most materials, previous studies have demonstrated similar anisotropic behaviour of fish skin [29,30]. For these reasons only results along the head–tail axis are presented. This effect, associated with strong anisotropy, was not

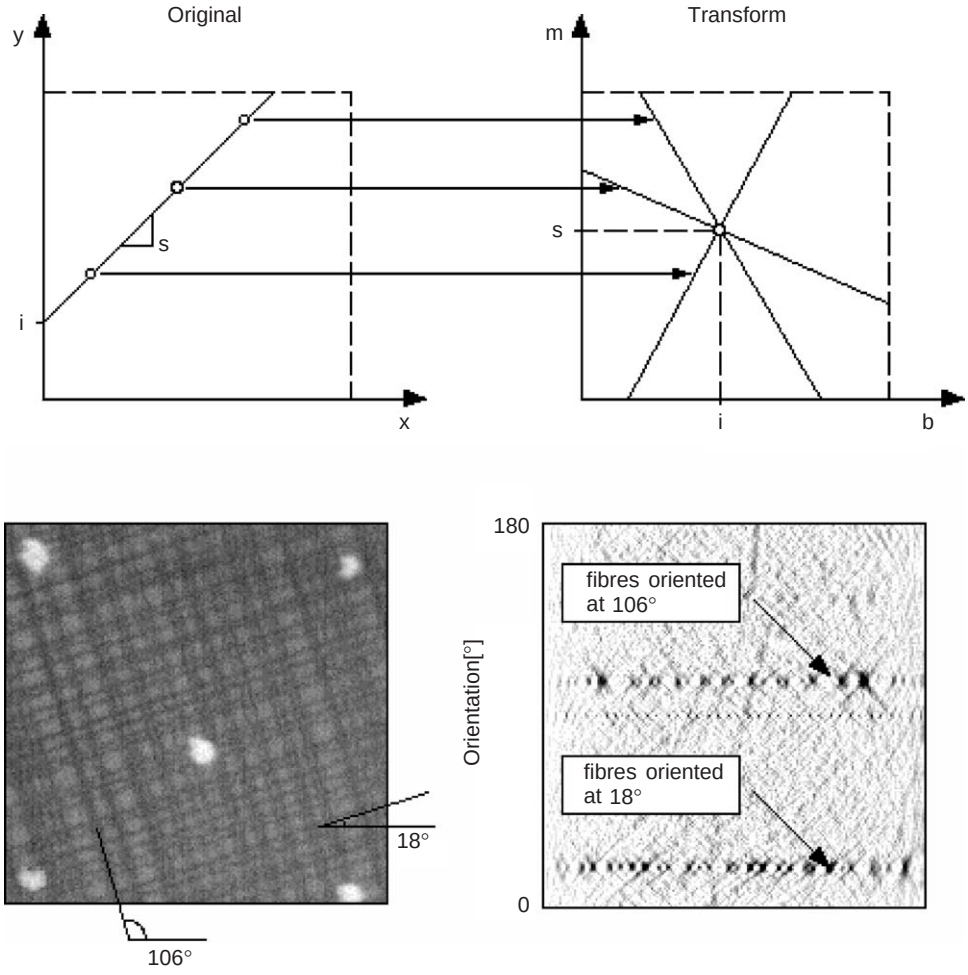

Fig. 2. The Hough Transform is demonstrated by displaying an original image and its corresponding transform. On the top, left is the original image with a straight line defined by three points. The transformed image (top, right) represents these points by a family of lines that intersect at the slope (m) and intercept (b) of the original line. The Hough Transform applied to a single captured frame during deformation of the model textile materials is shown below. The original captured frame (bottom, left) is the central portion of the textile laminate bounded by the locations of surface deformation markers shown in white. The corresponding Hough Transform (bottom, right) illustrates each fibre as a blackened circle. Each fibre population (orientated at 106° and 18°, respectively) is represented by a series of circles at the same vertical position.

observed in either of the other materials used in this study.

Fish skin samples became apparently less extensible and stiffer with decreasing arm length in the head–tail direction. The changes in maximum normal strain and modulus were significant with respect to sample arm length (Tables 1 and 2, respectively). This observation was readily apparent upon comparison of the averaged stress–strain curves (Fig. 3). The shear behaviour was not dramatically altered in these samples with only the maximum shear stress decreasing with decreasing arm length (Table 3). Rigid body rotation results were similar to shear stress results: a reduction in rotation with decreasing arm length (Table 4). Multiple comparisons revealed that, for all parameters except the modulus, the observed differences between arm lengths were not significant between 44 and 22 mm arm lengths.

3.2. Bovine pericardium

Upon the changes in sample geometry, the bovine pericardial samples displayed similar trends to the fish skin: an apparent reduction in extensibility and an increase in modulus with decreasing arm length. Both the maximum normal strain and modulus were significantly affected by sample arm length (Tables 1 and 2, respectively). Again, this effect was readily apparent upon comparison of average stress–strain curves (Fig. 4). The shear behaviour and the rigid body rotation changes were also very similar to the fish skin, both effects diminishing with decreasing arm length (Tables 3 and 4). Multiple comparisons of all parameters revealed that the behaviour of the 60 and 44 mm arm length samples were not significantly different from one another. For all sample geometries,

Table 1
Extensibility

	Arm length		
	60 mm	44 mm	22 mm
Fish skin			
H-T (E_{11})	0.11±0.010*	0.063±0.008	0.044±0.006
Bovine pericardium			
Circ. (E_{11})	0.22±0.020	0.22±0.021	0.10±0.011*
B-A (E_{22})	0.15±0.013	0.13±0.011	0.086±0.009*
Model materials			
E_{11}	0.005±0.001	0.007±0.001	0.007±0.001
E_{22}	0.005±0.001	0.003±0.001	0.001±0.000

The sample extensibility (defined as the valley-to-peak Green strain components E_{11} and E_{22}) are displayed as a function of cruciform sample arm length, for the each of the materials tested. Results shown as mean±standard error.
*Value denotes a significant difference with all other arm length groups ($p<0.02$).
Fish skin ($n=16$), bovine pericardium ($n=8$), and model textile materials ($n=8$).

Table 2
Modulus

	Arm length		
	60 mm	44 mm	22 mm
Fish skin			
H-T	1.6±0.49	1.8±0.11	3.8±0.70*
Bovine pericardium			
Circ.	3.3±0.52	5.0±0.89***	5.6±0.37**
B-A	4.2±0.64	7±1.6***	5.3±0.48
Model materials			
Axis 1	145±32	168±34	113±18
Axis 2	99±25	102±15	100±13

The tangent moduli are displayed as a function of cruciform sample arm length, for the each of the materials tested. Presented moduli reflect those determined approximately half way up the loading curve of the average deformation cycles for comparison purposes only (fish skin: 40 kPa; bovine pericardium: 80 kPa; model textile laminates: 300 kPa). All results are displayed in MPa and presented as mean± ⊖ standard error.
*Value denotes a significant difference with all other arm length groups ($p<0.05$).
**Value denotes a significant difference between the 60 and 22 mm groups ($p<0.02$).
***Value denotes a trend between the 60 and the 44 mm groups ($p=0.06$).
Fish skin ($n=16$), bovine pericardium ($n=8$), and model textile materials ($n=8$).

it was also generally observed that the circumferential direction was less stiff and more extensible than the base-to-apex direction.

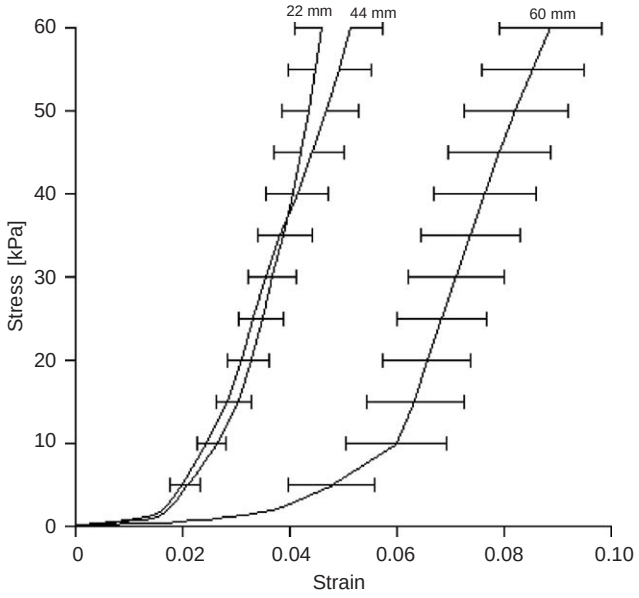

Fig. 3. Average stress–strain curves for the head–tail direction in fish skin are displayed for each sample arm length ($n=16$). Note that there were no differences in the behaviour between the 44 and 22 mm arm length samples. Only the loading curves are shown for clarity and the error bars represent the standard error of the mean strain.

3.3. Model textile laminates

For the model textile laminates, the only significant changes in material behaviour observed upon shortening the sample arms were in the shearing of the sample and in the rigid body rotation experienced during deformation. The maximum shear stress and shear strain, as well as the rigid body rotation, were reduced with decreasing sample arm length (Tables 3 and 4, respectively).

Upon visual inspection of the captured video images, two very different zones of deformation occurred in the model textile laminates (Fig. 5). The sample arms appeared to be compliant and underwent large deformations. The deformation that typically occurred within this region, although was not measured explicitly, was estimated to be 5–7 times larger than that occurring at the sample centre. A central zone oriented along the principal fibre directions appeared to be highly constrained, with only small deformations occurring. This zone also appeared to rotate towards the direction of stretch rather than to deform. The magnitude of this rotation was quantified through calculation of the rigid body rotation tensor. Measurement of individual fibre population rotations were quantified using the Hough transform and revealed that the two fibre populations tended to rotate in phase with one another with little inter-fibre shearing. Although a significant difference existed between the rotation results for each fibre population direction ($p<0.02$), the rigid body rotation of the sample centre was not different than either of the fibre population rotations (Table 4, $p>0.05$). Thus, in

Table 3
Shear behaviour

	Arm length		
	60 mm	44 mm	22 mm
Fish skin			
E_{12}	0.008±0.002***	0.005±0.001	0.004±0.001
S_{12} (kPa)	2.6±0.7*	0.8±0.2	1.0±0.2
S_{21} (kPa)	3.3±0.7*	1.5±0.2	1.1±0.2
Bovine pericardium			
E_{12}	0.022±0.009	0.024±0.007	0.004±0.001*
S_{12} (kPa)	6.8±1.6	4.0±0.6	0.9±0.2*
S_{21} (kPa)	7.0±0.9	5.9±1.6	1.9±0.7*
Model materials			
E_{12}	0.005±0.001**	0.003±0.001	0.001±0.001
S_{12} (kPa)	18±2.1*	10±1.9*	3.0±1.2*
S_{21} (kPa)	15±1.2*	7.3±1.1*	1.7±0.4*

The maximum shear strain (defined as the valley-to-peak Green strain component E_{12}) and maximum shear stress (defined as the valley-to-peak Kirchhoff stress components S_{12} and S_{21}) are displayed as a function of cruciform sample arm length, for the each of the materials tested. Results shown as mean±standard error.
*Value denotes a significant difference with all other arm length groups ($p<0.05$).
**Value denotes a significant difference between the 60 mm and the 22 mm groups ($p<0.05$).
***Value denotes a trend between the 60 and 22 mm arm length groups ($p=0.10$).
Fish skin ($n=16$), bovine pericardium ($n=8$), and model textile materials ($n=8$).

Table 4
Rigid body and fibre rotation results

	Arm length		
	60 mm	44 mm	22 mm
Fish skin	0.9±0.19**	0.42±0.05	0.36±0.06
Bovine pericardium	1.5±0.12	1.1±0.17	0.19±0.039*
Model materials†	2.4±0.14*	1.2±0.16*	0.18±0.053*
Fibre population 1	2.1±0.11*	1.0±0.11*	0.1±0.05*
Fibre population 2	2.6±0.24*	1.5±0.16*	0.2±0.14*

The maximum rigid body rotation were determined as the difference between the valley and peak values and are presented as a function of cruciform sample arm length, for the each of the materials tested. Maximum rotations of fibres (for each fibre population) in the model textile materials were determined using the Hough Transform. All results are displayed in degrees (°) and presented as mean±standard error.
*Value denotes a significant difference with all other arm length groups ($p<0.05$).
**Value denotes a trend between the 60 and the 22 mm groups ($p=0.08$).
†Denotes a significant difference between both fibre populations ($p<0.02$).
Fish skin ($n=16$), bovine pericardium ($n=8$), and model textile materials ($n=8$).

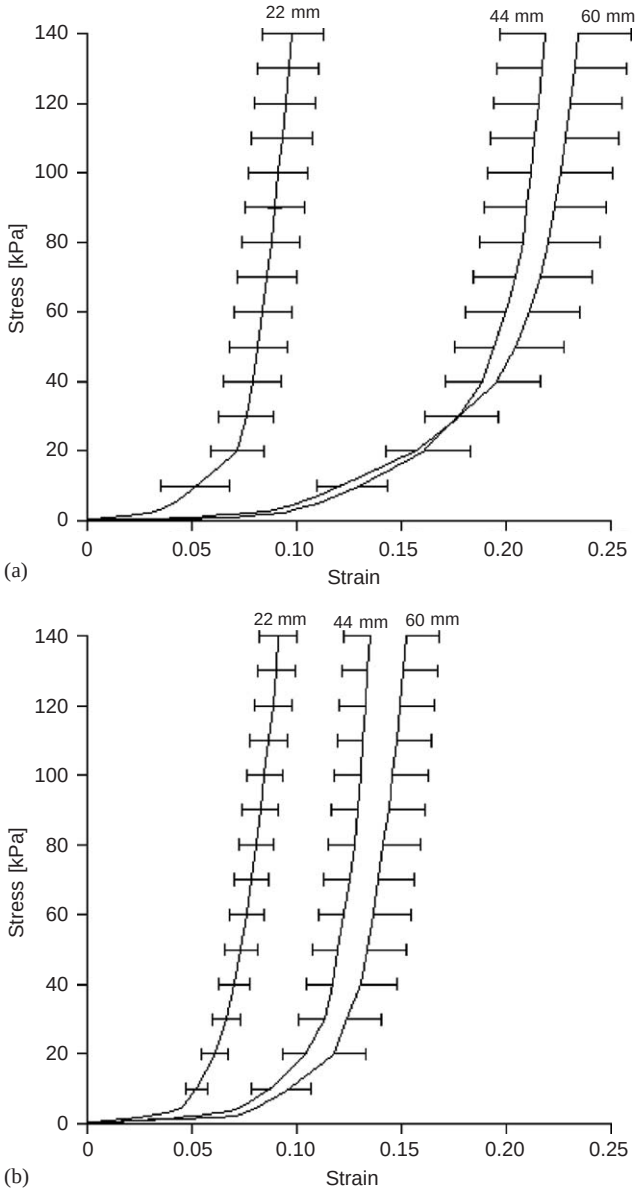

Fig. 4. Average stress–strain curves for the circumferential direction (a) and the base-to-apex direction (b) of bovine pericardium are displayed for each sample arm length ($n=8$). Note that there were no differences in the behaviour between the 60 and 44 mm arm length samples in either direction. Only the loading curves are shown for clarity and the errors bars represent standard error of the mean strain.

this case, the rigid body rotation represents an average measure of actual fibre rotation. All measures of rotation (fibre rotation and sample rigid body rotation) were dependent on sample arm length with less rotation observed in shorter arm length samples.

4. Discussion

This study demonstrates that the observed mechanical behaviour of planar connective tissues under biaxial

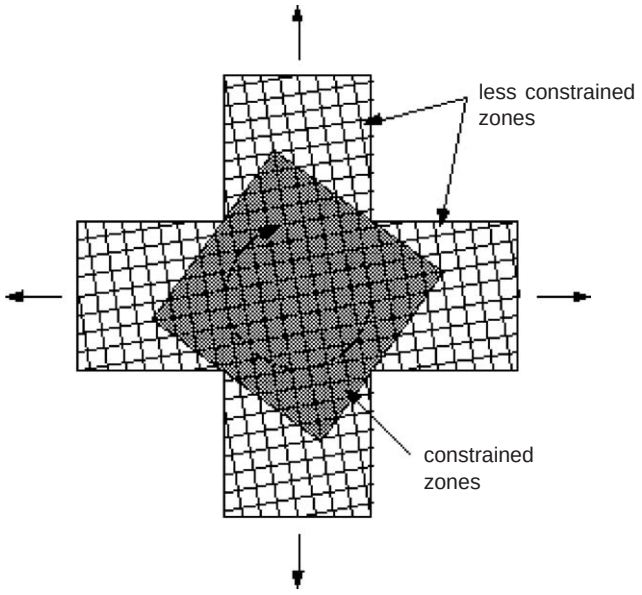

Fig. 5. Two distinct zones of deformation occurred in the model textile materials upon visual inspection of the captured video images. The central portion of the sample (darkened region in the figure) appeared to be more constrained than the outer arms. This region was bounded by the principal fibre directions and tended to rotate towards the direction of stretch rather than to deform.

loading is dependent on the test sample geometry. With mechanical properties determined at the sample centre, cruciform-shaped samples became *apparently* stiffer and less extensible with decreasing sample aspect ratio. Dramatic changes in the amount of sample shearing and rigid body rotation of sample centre were also noted. These results may be attributed to alterations in the constraint on the underlying fibres since the same sample was tested with varying geometries. As the sample arms were shortened, more fibres were recruited into the mechanical response since a greater proportion of fibres were completely contained within the grips. This resulted in a direct increase in the observed modulus of the material, as well as a decrease in the amount of extension experienced under a particular load.

Striking similarities in the measured shear behaviour and rigid body rotation were observed between the model textile laminates and the connective tissues. All materials displayed a reduction in the amount of sample shearing and rigid body rotation with shorter cruciform sample arms. For the model textile materials, an analysis of the deformation pattern of the entire sample (from recorded video segments) revealed a potential mechanism to explain these observations. As stated previously, two different zones of deformation occurred within the sample. The sample arms underwent large deformations whereas a centralized region, defined by the principal fibre directions, tended to rotate towards the direction of stretch rather than to deform. The convergence of the four arms at the sample centre created a biaxial constraint in this region. Although constrained, the central portion was not fixed in space by the grips and thus was free to rotate. The sample arms, however, were only subject to a uniaxial constraint. This encouraged the bulk of deformation to occur there versus in the highly constrained centre. Since the fibres were not originally symmetrically oriented about the material test axes, the stretching of the sample arms produced a force couple on each fibre within the central region. Addition of the all the force couples created a net moment that rotated the centre of the sample towards the direction of stretch (Fig. 5). As the sample arm lengths were shortened, the material within this region became apparently stiffer presumably due to a larger proportion of fibres being completely contained within the grips. Under the same loading, less deformation occurred within the arms—ultimately resulting in lower rotations at the sample centre. For the same reason, any non-symmetrical fibre arrangement about the material test axes should produce a centralized sample rotation towards the direction of stretch under equibiaxial loading. This rotation, however, would be minimized if the material axes were initially aligned with the testing axes (assuming that the material had a well-defined, symmetrical fibre distribution). To our knowledge this rigid rotational effect has not been reported before in planar connective tissues during in vitro mechanical testing. There has been, however, an observation of rigid body rotation of the epicardium in vivo [51]: a phenomenon attributed by those authors to the torsional deformation of the ventricle during normal cardiac function.

Also, since the fibres were not aligned with the testing axes, some degree of sample shearing would be expected. Indeed, this was observed. More importantly, with shorter sample arms, the increasing fibre containment within the grips resulted in (i) increased constraint on the sample, thereby (ii) reducing the amount of shearing under the same load. The connective tissues samples (both fish skin and bovine pericardium) showed the same trends in the measured shearing behaviour with the applied changes in sample geometry, suggesting that a common deformation mechanism most likely occurred in the connective tissues and the model textile laminates.

Another explanation for the apparent differences in mechanical behaviour upon shortening the sample arms was the possibility of edge-related artifacts (i.e. Saint-Venant effect). The close proximity of the grips could have resulted in an apparent stiffening of the material—as commonly observed during uniaxial testing [23]. Although similar behaviour was noted in this study, the Saint-Venant effect has yet to be adequately demonstrated during biaxial material testing. The uniformity of biaxial strain-field was assessed to determine the

magnitude of edge-related effects [49,50] (variance in strain-field measurements was less than 20% in all samples) and no significant effects of the alterations in sample arm length were observed. This suggests that the alterations in material behaviour were not due to edge-related artifacts (Saint-Venant effect) as the sample arms were shortened and another mechanism is responsible such as the amount of extracellular fibres that were effectively contained grip-to-grip.

Apart from the observed changes in the apparent biaxial mechanical behaviour with altered sample geometry, the general biaxial behaviour of connective tissue samples were consistent with previous studies. The head-tail direction was dramatically more extensible than the dorsal-ventral direction for various species of fish (norfolk spot, skipjack tuna, and lemon shark) [29,30]. For the pericardium, similar observations of reduced extensibility and increased stiffness of the base–apex direction have also been noted in the literature [5,6,52–54].

Although the majority of biaxial tests on connective tissues to date have utilized sutured-square samples, the present study focused on the cruciform sample with clamped edges. The cruciform sample has deep roots in biaxial material testing and is the sample geometry of choice for engineering composite materials. Planar connective tissues can be thought of as biological composites and thus this method should warrant investigation. Our study, however, suggests that the use of cruciform samples for connective tissue testing may not be favourable since material properties were highly dependent on sample arm length; nonetheless, there is no guarantee that the common methodology of suturing sample edges is superior. Suturing sample edges might result in a discontinuous load transfer to the underlying fibrous network since only discrete groups of fibres within the vicinity of the suture attachment point are loaded [55]. The number and position of suture attachment points should therefore also have an affect on the mechanical properties of the sample. Indeed, there seems to be no consensus on the optimum number of suture attachment points. We have found a wide variability in the literature ranging from four [56] to ten [57] suture attachment points per sample side.

The results of this study, shed light on a broader issue, that any properties measured in vitro have a degree of artifactual behaviour associated with them. The only truly reliable method to determine material properties is through in vivo testing, but this is not always convenient and is typically experimentally demanding. In order to minimize testing artifacts during the in vitro determination of the biaxial material properties, samples should be created to ensure that the majoirty of the extracellular reinfoircing fibres are effectively contained with the grips. The common use of orienting samples with respect to their anatomical directions alone to is not sufficient to provide this preferred orientation and can lead to the inaccuracte determination of material behaviour and properties. Although there exist methods to non-destructively assess extracellular fibre orientations prior to mechanical testing [58,59], they have only proven useful for highly collagenous materials.

Acknowledgements

This work was supported by a grant from the Natural Sciences and Engineering Research Council (NSERC) and a student fellowship from the Heart and Stroke Foundation of Canada (HSFC). Model textile materials were created with the support of Mr. Gordon Hall and Dr. Derek Jones, Faculty of Dentistry, Dalhousie University. Surface marker isolation and tracking video analysis macros in NIH Image were developed by Mr. Rajesh Khanna. The public domain NIH Image program (US National Institutes of Health) is available from the Internet by anonymous FTP from ⟨zippy.nimh.nih.gov⟩.

References

[1] Hildebrant J, Fukaya H, Martin CJ. Stress–strain relations of tissue sheets undergoing uniform two-dimensional stretch. J Appl Physiol 1969;27:758–62.
[2] Barbenel JC, Zioupos P, Fisher J. In: Barbenel JC, editor. Blood flow in artificial organs and cardiovascular prostheses. Oxford: Clarendon Press; 1989. p. 31–4.
[3] Zioupos P, Barbenel JC, Fisher J. Mechanical and optical anisotropy of bovine pericardium. Med Biol Eng Comput 1992; 30:76–82.
[4] Lanir L, Fung YC. Two-dimensional properties of rabbit skin. 2. Experimental results. J Biomech 1974;7:171–82.
[5] Lee MC, LeWinter MM, Freeman G, Shabetai R, Fung YC. Biaxial mechanical behavior of the pericardium in normal and volume overloaded dogs. Am J Physiol 1985;249:H222–30.
[6] Lee MC, Fung YC, Shabetai R, LeWinter MM. Biaxial mechanical properties of human pericardium and canine comparisons. Am J Physiol 1987;253:H75–82.
[7] Humphrey JD, Vawter DL, Vito RP. Pseudoelasticity of excised visceral pleura. J Biomech Eng 1987;109:115–20.
[8] Humphrey JD, Strumpf RK, Yin FCP. Biaxial mechanical behavior of excised ventricular epicardium. Am J Physiol 1990; 259:H101–8.
[9] Humphrey JD, Strumpf RK, Yin FCP. Determination of a constitutive relation for passive myocardium. 1. A new functional form. J Biomech Eng 1990;112:333–9.
[10] Mönch E, Galster D. A method for producing a defined uniform biaxial tensile stress field. Br J Appl Phys 1963;14:810–2.
[11] Kreissig R, Schindler J. Some experimental results on the yield condition in plane-stress state. Acta Mech 1986;65:169–79.
[12] Kashiwaya K. Fundamentals of nondestructive measurement of biaxial stress in steel utilizing magnetoelastic effect under low magnetic-field. Jpn J Appl Phys 1991;30:2932–42.
[13] Hjelm HE. Yield surface for gray cast iron on biaxial stress. J Eng Mater Tech; Trans ASME 1994;116:148–54.
[14] Bert CW, Mayberry BL, Ray JD. Behavior of fiber-reinforced plastic laminates under biaxial loading. In: Composite materials:

testing and design, ASTM STP 460. American Society for Testing and Materials, 1969. p. 362–380.
[15] Daniel IM. In: Test methods and design allowables for fibrous composites, ASTM STP 734. American Society for Testing and Materials, 1981. p. 109–124.
[16] Fawaz Z, Neale KW. A cruciform specimen for the evaluation of biaxial properties of advanced composites. Trans CSME 1995; 19:25.
[17] Tandon GP, Kim RY, Bechel VT. Fiber-matrix interfacial failure characterization using a cruciform-shaped specimen. J Comput Mater 2002;36:2667–91.
[18] Boisse P, Borr M, Buet K, Cherouat A. Finite element simulations of textile composite forming including the biaxial fabric behaviour. Composites Part B 1997;28B:453–64.
[19] Flynn DM, Peura GD, Grigg P, Hoffman AH. A finite element based method to determine the properties of planar soft tissue. J Biomech Eng 1998;120:202–10.
[20] Langdon SE, Chernecky R, Pereira CA, Abdulla D, Lee JM. Biaxial mechanical/structural effects of equibiaxial strain during crosslinking of bovine pericardial xenograft materials. Biomaterials 1999;20:137–53.
[21] Butler DL, Grood ES, Noyes FR, Zernicke RF, Brackett K. Effects of structure and strain-measurement technique on the material properties of young human tendons and fascia. J Biomech 1984;17:579–96.
[22] Zernicke RF, Butler DL, Grood ES, Hefzy MS. Strain topography of human tendon and fascia. J Biomech Eng 1984;106:177–80.
[23] Jimenez ML, Brown TD, Brand RA. The effects of grip proximity on perceived local in vitro tendon strain. J Biomech 1989;22:949–55.
[24] Ishihara T, Ferrans VJ, Boyce SW, Jones M, Kawanami O, Roberts WC. Histologic and ultrastructural features of normal human parietal pericardium. Am J Cardiol 1980;46: 744–53.
[25] Ishihara T, Ferrans VJ, Jones M, Boyce SW, Roberts WC. Structure of bovine parietal pericardium and of un-implanted ionescu-shiley pericardial valvular bioprostheses. J Thorac Cardiovasc Surg 1981;81:747–57.
[26] Wiegner AW, Bing OHL, Borg TK, Caulfield JB. mechanical and structural correlates of canine pericardium. Circ Res 1981;49: 807–14.
[27] Naimark WA, Lee JM, Limeback H, Cheung DT. Correlation of structure and viscoelastic properties in the pericardia of four mammalian-species. Am J Physiol 1992;263:H1095–106.
[28] Wallraff J. Herzbeutels Klin Wochenschr 1937;16:1665–9.
[29] Hebrank MR, Hebrank JH. The mechanics of fish skin—lack of an external tendon role in two teleosts. Biol Bull 1986;171:236–47.
[30] Wainwright SA, Vosburgh F, Hebrank JH. Shark skin—function in locomotion. Science 1978;202:747–9.
[31] Nadol Jr. JB, Gibbins JR, Porter KR. A reinterpretation of structure and development of basement lamella—an ordered array of collagen in fish skin. Dev Biol 1969;20:304–31.
[32] Trotter JA, Koob TJ. Collagen and proteoglycan in a sea-urchin ligament with mutable mechanical-properties. Cell Tissue Res 1989;258:527–39.
[33] Birk DE, Nurminskaya MV, Zycband EI. Collagen fibrillogenesis in-situ—fibril segments undergo postdepositional modifications resulting in linear and lateral growth during matrix development. Dev Dyn 1995;202:229–43.
[34] Birk DE, Zycband EI, Woodruff S, Winkelmann DA, Trelstad RL. Collagen fibrillogenesis in situ: Fibril segments become long fibrils as the developing tendon matures. Dev Dyn 1997;208: 291–8.
[35] Silver FH, Kato YP, Ohno M, Wasserman AJ. Analysis of mammalian connective-tissue—relationship between hierarchical structures and mechanical-properties. J Long-Term Eff Med Implants 1992;2:165–98.
[36] Cribb AM, Scott JE. Tendon response to tensile-stress—an ultrastructural investigation of collagen—proteoglycan interactions in stressed tendon. J Anat 1995;187:423–8.
[37] Sanjeevi R, Somanathan N, Ramaswamy D. A viscoelastic model for collagen-fibers. J Biomech 1982;15:181–3.
[38] Haut RC. The influence of specimen length on the tensile failure properties of tendon collagen. J Biomech 1986;19:951–5.
[39] Hawkes JW. Structure of fish skin. 1. General organization. Cell Tissue Res 1974;149:147–58.
[40] Elias H, Boyd LJ. Notes on the anatomy, embryology, and histology of the pericardium. J NY Med Coll 1960;2:50–75.
[41] Kluge T, Hovig T. Ultrastructure of human and rat pericardium. 1. Parietal and visceral mesothelium. Acta Pathol Microbiol Scand 1967;71:529–46.
[42] Lee JM, Langdon SE. Thickness measurement of soft tissue biomaterials: a comparison of five methods. J Biomech 1996;29: 829–32.
[43] Hoffman AH, Grigg P. A method for measuring strains in soft-tissue. J Biomech 1984;17:795–800.
[44] McCulloch AD, Omens JH. Nonhomogeneous analysis of three-dimensional transmural finite deformation in canine ventricular myocardium. J Biomech 1991;24:539–48.
[45] Green AE. Large elastic deformations. New York: Claredon Press (2nd edition); 1970.
[46] Fung YC. Biomechanics: mechanical properties of living tissues. New York: Springer; 1981.
[47] Malvern LE. Introduction to the mechanics of a continuous medium. Englewood Cliffs, NJ: Prentice-Hall; 1969.
[48] Duda RO, Hart PE. Use of Hough transformation to detect lines and curves in pictures. Commun ACM 1972;15:11–5.
[49] Humphrey JD, Vawter DL, Vito RP. Quantification of strains in biaxially tested soft-tissues. J Biomech 1987;20:59–65.
[50] Nielsen PMF, Hunter PJ, Smaill BH. Biaxial testing of membrane biomaterials—testing equipment and procedures. J Biomech Eng 1991;113:295–300.
[51] McCulloch AD, Smaill BH, Hunter PJ. Regional left-ventricular epicardial deformation in the passive-dog heart. Circ Res 1989;64: 721–33.
[52] Chew PH, Yin FCP, Zeger SL. Biaxial stress–strain properties of canine pericardium. J Mol Cell Cardiol 1986;18:567–78.
[53] Lee JM, Haberer SA, Boughner DR. The bovine pericardial xenograft. 1. Effect of fixation in aldehydes without constraint on the tensile viscoelastic properties of bovine pericardium. J Biomed Mater Res 1989;23:457–75.
[54] Choi HS, Vito RP. Two-dimensional stress–strain relationship for canine pericardium. J Biomech Eng 1990;112:153–9.
[55] Waldman SD, Sacks MS, Lee JM. Boundary conditions during biaxial testing of planar connective tissues. Part II—Fiber orientation. J Mater Sci Lett 2002;21:1215–21.
[56] Gupta KB, Ratcliffe MB, Fallert MA, Edmunds Jr. LH, Bogen DK. Changes in passive mechanical stiffness of myocardial tissue with aneurysm formation. Circulation 1994;89:2315–26.
[57] Schneider DC, Davidson TM, Nahum AM. In vitro biaxial stress-strain response of human skin. Arch Otolaryngol 1984;110: 329–33.
[58] Sacks MS, Chuong CJ. Characterization of collagen fiber architecture in the canine diaphragmatic central tendon. J Biomech Eng 1992;114(2):183–90.
[59] Sacks MS, Chuong CJ, More R. Collagen fiber architecture of bovine pericardium. ASAIO J 1994;40(3):M632–7.